Dyes and Pigments 219 (2023) 111610

Contents lists available at ScienceDirect

Dyes and Pigments

journal homepage: www.elsevier.com/locate/dyepig

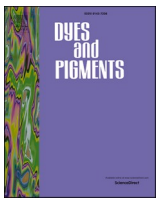

Chromogenic azomacrocycles with imidazole residue: Structure vs. properties

Błażej Galiński [a], Jarosław Chojnacki [b], Katarzyna Szwarc-Karabyka [c], Adrian Małkowski [a,1], Diana Sopel [a,1], Agnieszka Zwolińska [a,1], Ewa Wagner-Wysiecka [a,d,*]

[a] Department of Chemistry and Technology of Functional Materials, Faculty of Chemistry, Gdańsk University of Technology, Narutowicza Street 11/12, 80-233, Gdańsk, Poland
[b] Department of Inorganic Chemistry, Faculty of Chemistry, Gdańsk University of Technology, Narutowicza Street 11/12, 80-233, Gdańsk, Poland
[c] Nuclear Magnetic Resonance Laboratory, Faculty of Chemistry, Gdańsk University of Technology, Narutowicza Street 11/12, 80-233, Gdańsk, Poland
[d] Advanced Materials Center, Faculty of Chemistry, Gdańsk University of Technology, Narutowicza Street 11/12, 80-233, Gdańsk, Poland

ARTICLE INFO

Keywords:
Azocompound
X-ray analysis
Colorimetric sensor
Porous glass
Smartphone

ABSTRACT

New diazo macrocycles linked by hydrocarbon chain bearing imidazole or 4-methylimidazole residue have been synthetized with satisfactory yield (24–55%). The structure of macrocycles was confirmed by X-ray analysis and spectroscopic methods (^{1}H NMR, MS, FTIR). Metal cation complexation studies were carried out in acetonitrile and acetonitrile-water system. It was found that azomacrocyles form triple-decker complexes with lead(II). The highest values of stability constant were found for lead(II) complexes of 21-membered derivatives. For the first time azomacrocycles bearing imidazole residue were immobilized on a porous glass. Obtained materials can act as lead(II) or copper(II) colorimetric optical sensors with color digital analysis as detection using simple portable devices.

1. Introduction

The presence of harmful compounds including heavy metals in food, such as fish, vegetables and fruit, associated with increasing environmental pollution is an ever-growing global problem [1–3]. Water is an essential nutrient and the most important solvent for living organisms. Its availability is decreasing and its pollution is increasing [4]. Pollution of water, soil [5–8] and air [9–12], causes accumulation of hazardous metals in aqueous systems [13], and animal [14] and plant organisms [15]. Consumption of contaminated food is associated with frequent poisoning as well as dangerous diseases caused by the accumulation of heavy metals in the human body [16–21]. Some heavy metals such as chromium, manganese, nickel, zinc, iron or copper are key elements necessary for the proper functioning of the human body, however, also their elevated levels are dangerous for health and life [22,23]. On the other hand, heavy metals such as lead, cadmium, mercury or arsenic pose a serious ecological threat and are toxic to living organisms and their accumulation may result in kidney dysfunction, brain tumors and metabolic disorders [24]. Early and rapid detection of elevated levels of heavy metals and other harmful compounds in biological and environmental samples is of great importance and crucial in maintaining health [25]. Valuable analytical tools which can be used for this purpose are optical sensors which serve fast and reliable detection/determination of analytes of different nature [26–33]. Constantly popular are chemical optical sensors, including optodes, due to their simplicity and possibility of non-instrumental detection, i.e. detection and determination with the naked eye, as well as low hardware requirements [34–37]. Receptor layers of optical sensors are characterized by relatively high sensitivity and selectivity, relatively simple and low cost preparation and relatively fast response time [38–41]. Optical sensors allow determination of many chemical species of different properties and chemical nature, depending on the receptor layers used. Among various solutions of preparation of optical sensor layers porous glasses can be used for the immobilization chromo(fluoro)ionophores. Comparing, for example polymeric matrix often used in classical optodes, such materials offer the photochemical and thermal stability, which is limited by the duration of the chromoionophore and the rest of the components (plasticizer, ionic additives etc.) of the layer [42]. Among the others, colorimetric and fluorescent

* Corresponding author.Department of Chemistry and Technology of Functional Materials, Faculty of Chemistry, Gdańsk University of Technology, Narutowicza Street 11/12, 80-233, Gdańsk, Poland.
E-mail address: ewa.wagner-wysiecka@pg.edu.pl (E. Wagner-Wysiecka).
[1] authors of the same degree of contribution given in alphabetical order.

https://doi.org/10.1016/j.dyepig.2023.111610
Received 25 June 2023; Received in revised form 1 August 2023; Accepted 7 August 2023
Available online 8 August 2023

pH sensors using covalently immobilized pH indicators onto porous glasses were obtained [43–46]. Porous matrix materials were also interest as optical sensing of gaseous oxygen [47]. The advantage is the longer life time of sensing material comparing materials where physical immobilization is used. However the weak point is the preparation of the sensing layer, which usually needs a multi step preparation protocol.

Large group of the optical sensors is based on supramolecular approach, where in the sensor matrix selective towards a particular analyte (guest) host molecule is immobilized. Among such solutions interesting are those which use chromogenic receptors. It differs from traditional optodes for which the most often solution is using ionophore responsible for analyte recognition and chromophore (usually acid-base indicator) thanks to which the optical signal is generated. One of the advantages of such an approach is the limitation of the chemical components of the sensing layer. Among colored metal ion receptors large group of effective chromionophores constitute azo compounds [48,49] and among them macrocylic azo derivatives [50,51]. Application of well-designed macrocylic receptors discriminating metal ions according to their size can significantly improve selectivity of optical sensors. However the synthesis of the macrocyclic compounds is often laborious and challenging [52–54]. Among chromogenic macrocyclic compounds an interesting group of are molecules with two azo groups and heterocyclic moiety constituting a part of macroring. Compounds of this type have been obtained in our group in relatively facile synthetic protocols with satisfactory yields [55–61]. The high selectivity towards metal cations enabled using macrocyclic pyrrole derivatives as ionophores in lead(II) selective ion-selective electrodes [56] and optodes [61]. Macrocyclic derivatives bearing imidazole moiety as a part of macrocycle have been also investigated as ionophores in membrane ion-selective electrodes [59]. Some macrocyclic imidazole derivatives were encapsulated in silica xerogel matrices and proposed as optical chemical recognition elements [62].

Promising results obtained for optodes based on macrocyclic pyrrole derivatives [61] have encouraged us to study the influence of the type of heterocyclic moiety on selectivity of the chromogenic receptor layers towards metal ions. Therefore, the aim of the work is to investigate the properties of macrocyclic imidazole derivatives as chromoionphores and to determine their possible use in the receptor layers of optical sensors. New macrocyclic derivatives of imidazole and 4-methylimidazole besides previously obtained were also synthetized for the purposes of this study. Moreover, the goal of this paper is the assessment of the application of the porous glass as solid support for chromoionophore immobilization – as easy and non-labor and non-time consuming user friendly optical sensors with digital color analysis used as detection mode.

2. Experimental

2.1. Materials

All chemicals of the highest available purity were purchased from commercial sources and used without further purification. For metal cation complexation, lithium perchlorate (99.9%, Sigma Aldrich), sodium perchlorate monohydrate (>99.0%, Fluka), potassium perchlorate (>99.0%, Sigma Aldrich), magnesium perchlorate (≤100%, Alfa Aesar), calcium perchlorate tetrahydrate (99.0%, Alfa Aesar), strontium perchlorate trihydrate (≤100%, Alfa Aesar), barium perchlorate (97.0%, Sigma Aldrich), cobalt(II) perchlorate hexahydrate (98.0%, Sigma Aldrich), nickel(II) perchlorate hexahydrate (≥98.5%, Sigma Aldrich), copper(II) perchlorate hexahydrate (98.0%, Sigma Aldrich), zinc perchlorate hexahydrate (Sigma Aldrich), cadmium perchlorate hexahydrate (Alfa Aesar) and lead(II) perchlorate trihydrate (≥99.0%, Sigma Aldrich). For acid-base properties studies *p*-toluenesulfonic acid monohydrate (pure, POCH, Gliwice, Poland), tetra-*n*-butylammonium hydroxide 30-hydrate (98%, Sigma-Aldrich, Steinhaim, Germany) were used. Metal nitrates: sodium nitrate (≥99.8%, POCH), potassium nitrate (≥99.8%, POCH), magnesium nitrate hexahydrate (≥99.0%, POCH), calcium nitrate tetrahydrate (≥99.0%, POCH), strontium nitrate (≥99.0%, POCH), barium nitrate (≥99.0%, POCH), cobalt(II) nitrate hexahydrate (≥98.0%, POCH), nickel(II) nitrate hexahydrate (≥98.0%, POCH), copper(II) nitrate trihydrate (≥99.5%, Merck), zinc nitrate hexahydrate (≥98.0%, POCH), cadmium nitrate tetrahydrate (≥98.0%, POCH) and lead(II) nitrate (≥99.0%, Alfa Aesar). Porous glass (polystyrene modified, particle size 0.075–0.125 mm, $M_w \sim 120000$ Corning) was used for preparation of sensing layers. UV–Vis measurements were carried out in acetonitrile (spectroscopic-grade, Merck). All aqueous solutions were prepared using ultra-pure water obtained by the reverse osmosis (RO) from Hydrolab Poland station (conductivity <1 μS/cm^{-1}). For preparation of sensing layers dichloromethane (p.a. POCh) was used as a solvent. In synthetic protocols p.a. solvents were used. TLC plates 60 RP-18 F_{254} for lipophilicity determination, TLC plates 60 F_{254} for reaction progress tracing and determination of R_f parameters and silica gel 60 (0.063–0.200 mm) for column chromatography were purchased from Merck.

2.2. Instrumentation

^{1}H and ^{13}C NMR spectra were recorded on a Varian INOVA 500 spectrometer at 500 and at 125 MHz, respectively. Chemical shifts are reported in δ (ppm) units. FTIR spectra (ATR) were taken on the Nicolet iS10 apparatus. Mass spectra (LR and HRMS EI) were taken on a Autospec Premier (Waters) spectrometer. UV–Vis measurements were carried out in 1 cm quartz cuvettes with the use of an UNICAM UV 300 series spectrometer. The solution pH was measured by an pH-meter CPC-511 with glass electrode EPS-1 (ELMETRON), standardized with buffer solutions. Portable LED light box (23 × 23 × 23 cm) was used to guarantee the reproducibility of the photos (PULUZ, Photography Light Box, Shenzhen Puluz Technology Limited). The phone which camera was used for the photos was the Apple iPhone 7 Plus.

2.3. Synthesis of macrocycles 1–4

Macrocycles **1**–**4** were obtained by diazocoupling of diazonium salt with imidazole or 4-methylimidazole using synthetic protocols elaborated on our group [55–60]. The procedure of the synthesis and structural characterization of newly obtained macrocycles are given in Electronic Supplementary Information (ESI).

2.4. X-ray structure determination

Diffraction intensity data for **1**, **3**, **4** and **6** were collected on an IPDS 2T dual beam diffractometer (STOE & Cie GmbH, Darmstadt, Germany) at 120.0(2) K with MoKα radiation of a microfocus X-ray source (GeniX 3D Mo High Flux, Xenocs, Sassenage, 50 kV, 1.0 mA, and λ = 0.71069 Å). Investigated crystals were thermostated under a nitrogen stream at 120 K using the CryoStream-800 device (Oxford CryoSystem, UK) during the entire experiment.

Data collection and data reduction were controlled by using the X-Area 1.75 program (STOE, 2015). Due to low absorption coefficient no absorption correction was performed. The structures were solved using intrinsic phasing implemented in SHELXT and refined anisotropically using the program packages Olex2 [63] and SHELX-2015 [64]. Positions of the C–H hydrogen atoms were calculated geometrically taking into account isotropic temperature factors. All hydrocarbonic H-atoms were refined as riding on their parent atoms with the usual restraints. All NH atoms were found in the Fourier electron density map and refined with N–H bond length constrained to 0.86(2) Å.

Structure of **1** was solved in the space group $P2_1/c$ and refined without any special treatment. Structure **3** was refined with the assumption the electron density in the mean unit cell has higher symmetry than actual molecules. The mean electron density is an average of the molecule and its mirror reflection. Thus, the asymmetric unit, being

half of the molecule, contains N3–H3 and (C11–H11 and N4) and C9, H9A, H9B atoms with occupation factor equal to ½. It is worthy to add, that initially the solution was found in polar space group $Pna2_1$, but PLATON finds additional symmetry, leading to the reported solution in space group *Pnma*. In order to maintain numerical stability restrains of equal ellipsoids were applied to (half occupied) atoms N4 and C11, sharing the same positions.

Structure of **4** was solved in the space group $P2_1/c$ and refined without any special treatment.

Compound **5** crystallizes in the space group *I*2/*m* (No. 12, cell choice 3 of *C*2/*m*). Cell parameters: (*a, b, c* (Å); *α, β, γ* (°) = 7.7187 (17), 31.861 (9), 29.749 (6); 90, 94.805 (17), 90). The structure was solved, but not refined to a satisfactory quality and therefore it was not deposited in the Cambridge Database. Raw results indicate the asymmetric unit contains one regular macrocycle molecule and two halves of the two other, chemically identical, macrocycles, both having a mirror *m* symmetry. Each macrocyclic molecule is accompanied with a water molecule forming hydrogen bonding with an imidazole N-atom directed to the ring centre.

Structure of compound **6** was solved in the space group $P2_12_12_1$ and refined without any special treatment, but the absolute structure is uncertain since no heavy atom is present. Crystal data and structure refinement details for all crystal determined structures are collected in Table 1.

2.5. Structure determination in solution

The NMR spectra of **4** and **6** were recorded using a Varian INOVA 500 Spectrometer operating at 499.795 MHz in DMSO-d_6 solutions in ambient temperature. Chemical shifts are reported in δ (ppm) units using ^{1}H (residual) from DMSO-d_6 (2.49 ppm) as internal standard. 1D ^{1}H NMR spectra were collected with standard parameters (45° pulse length 3.9 μs and the delay time 1s). The 2D NMR spectra of **4** and **6** were recorded in ambient temperature. The ROESY spectrum was collected in the phase-sensitive mode with a spectral width of 5856 Hz and a mix time of 300 ms in a 4100 × 280 matrix with 16 accumulations per increment in a 4K × 1K matrix. The gHSQC and gHMBC experiments of all samples were performed with pulse field gradients. The gHSQC spectra were acquired in the phase-sensitive mode with ^{1}J(CH) set to 146 Hz. The spectral windows for ^{1}H and ^{13}C of axes were 5856 Hz and 20111 Hz, respectively. The data were collected with 64 accumulations per increment in a 1610 × 170 matrix and processed in a 2K × 2K matrix. The gHMBC spectra were acquired in absolute value mode with ^{n}J(CH) set to 8 Hz. The spectral windows for ^{1}H and ^{13}C of axes were 5856 Hz and 23881 Hz, respectively. The data were collected with 112 accumulations per increment in a 2620 × 170 matrix and processed in a 2K × 2K matrix.

2.6. Lipophilicity ($logP_{TLC}$)

The lipophilicity values of chromoionophores were determined by TLC method [48,60,66] using reversed phase RP18-TLC chromatography and mixture methanol:water (9:1, v/v) as a mobile phase. As standards BBPA, DBP, DOP, DOS and NPOE were used. $LogP_{TLC}$ values were determined by comparison of R_f values for standards and macrocycles.

Table 1
Crystal data and structure refinement details for all crystal structures determined.

Deposition No.	1	3	4	6
	2256005	2256006	2256007	2256008
Crystal data				
Chemical formula	$C_{19}H_{18}N_6O_2$	$C_{20}H_{20}N_6O_2$	$C_{21}H_{22}N_6O_2$	$C_{20}H_{20}N_6O_3$
M_r	362.39	376.42	390.44	392.42
Crystal system, space group	Monoclinic, $P2_1/c$	Orthorhombic, *Pnma*	Monoclinic, $P2_1/c$	Orthorhombic, $P2_12_12_1$
Temperature (K)	120	120	120	120
a, *b*, *c* (Å)	10.8716 (11), 7.0094 (4), 22.680 (2)	6.9729 (18), 15.911 (6), 16.167 (5)	15.677 (3), 11.0103 (16), 11.4065 (19)	4.0512 (3), 16.296 (2), 27.797 (3)
α, β, γ (°)	90, 91.818 (8), 90	90, 90, 90	90, 103.907 (13), 90	90, 90, 90
V (Å^3)	1727.4 (3)	1793.7 (10)	1911.2 (5)	1835.1 (4)
Z	4	4	4	4
Radiation type	Mo *K*α	Mo *K*α	Mo *K*α	Mo *K*α
μ (mm^{-1})	0.10	0.10	0.09	0.10
Crystal size (mm)	0.21 × 0.18 × 0.02	0.21 × 0.11 × 0.02	0.38 × 0.07 × 0.05	0.28 × 0.08 × 0.03
Data collection				
Diffractometer	STOE *IPDS* 2T	STOE *IPDS* 2T	STOE *IPDS* 2T	STOE *IPDS* 2T
Absorption correction	Multi-scan[a]	Multi-scan[a]	–	–
T_{min}, T_{max}	0.267, 0.997	0.444, 0.997	–	–
No. of measured, independent and observed [$I > 2\sigma(I)$] reflections	13715, 3050, 2007	12590, 2506, 2008	17724, 4175, 3395	7259, 2994, 1924
R_{int}	0.087	0.035	0.080	0.100
$(\sin\theta/\lambda)_{max}$ (Å^{-1})	0.595	0.691	0.639	0.580
Refinement				
$R[F^2 > 2\sigma(F^2)]$, $wR(F^2)$, *S*	0.073, 0.194, 1.13	0.039, 0.104, 1.01	0.068, 0.195, 1.03	0.107, 0.277, 1.16
No. of reflections	3050	2506	4175	2994
No. of parameters	248	130	266	264
No. of restraints	1	0	1	1
H-atom treatment	H atoms treated by a mixture of independent and constrained refinement	H-atom parameters constrained	H atoms treated by a mixture of independent and constrained refinement	H-atom parameters constrained
$\Delta\rho_{max}$, $\Delta\rho_{min}$ (e Å^{-3})	0.30, −0.38	0.28, −0.20	0.31, −0.35	0.34, −0.33
Absolute structure	–	–	–	Refined as an inversion twin.
Absolute structure parameter	–	–	–	0 (7)

[a] Multi-scan: STOE LANA, absorption correction by scaling of reflection intensities Afterwards a spherical absorption correction was performed within STOE LANA [65].

2.7. Metal cation complexation

Metal cation complexation studies were carried out using UV–Vis titration in acetonitrile and the mixture of acetonitrile with water. The stock solutions of macrocycles (~10^{-3} M), metal perchlorates (~10^{-2} M), TsOH (~10^{-2} M), TBAOH (~10^{-2} M) nitrates (~10^{-2} M), were prepared by weighting the respective quantities of them and dissolving in the respective solvent system in volumetric flasks. The values of binding constant (logK) were calculated with the use of OPIUM [67] program on the basis of titration experiment data.

2.8. Sensing layers preparation

Sensing materials based on porous glass (PG-PS) with different chromoionophore content (mg of chromoionophore per g of porous glass) were prepared using as working solutions of chromoionophores at a concentration of 0.1 mg/mL. Then 1.25, 2.5, 3.75 and 5 mL of solution was diluted to 10 mL with dichloromethane and next added to 500 mg of PG-PS to obtain sensing materials of 0.25, 0.5, 0.75 and 1 mg/g chromoionophore content per g of solid material. The mixture was stirred for 10 min and after that the mixture was transferred onto the Petri dish to evaporate solvent. The properties of the receptor layers were studied after immobilization using double-sided tape of the prepared material on 0.9 × 4.5 cm glass plates.

2.9. Measurement procedures-digital color analysis

Pictures of sensor layers were analyzed using free software ImageJ [68,69]. The change of optode color given as ΔE_{RGB} [48,61,70] was calculated using the equation: $\Delta E_{RGB} = [(R_0 - R)^2 + (G_0 - G)^2 + (B_0 - B)^2]^{1/2}$ where R_0, G_0 and B_0 values correspond to color of layer in the absence of metal salt, and R, G and B values correspond to color of layer in the presence of metal salt. Limits of detection (LOD) for copper (II) and lead(II) were calculated $DL = 10^{[(3\sigma - b)/a]}$, where σ is the standard deviation of the blank, b is intercept and a is the slope of the linear function ΔE_{RGB} = f(logarithm of molar concentration of analyte).

3. Results and discussion

3.1. Synthesis and characterization of macrocycles

New azomacrocycles **1**–**4** (Scheme 1) were obtained in analogous way as their oligoether analogs **5**–**8** [55,59]. The respective diazonium salt obtained from diamine **12** (or **13)** was diazocoupled with imidazole or 4-methylimidazole under high dilution conditions. In this way new 17- and 18-membered crowns **1**,**2** and **3**,**4** respectively were obtained.

It can be noted that macrocyclization yield for **1**–**4** is slightly higher for reactions where 4-methylimidazole was used as a substrate. Yields of compounds **1**–**4** linked by hydrocarbon chain are in general lower than for oligoether analogs **5**–**8**. Interestingly for oligoether linked compounds **5** and **7** bearing imidazole residue yields are higher than for macrocycles bearing 4-methylimidazole moiety. Yield of macrocyclization for compounds **1**–**8** is compared in Fig. 1. It can be stated that macrocyles with imidazole/4-methylimidazole rings are compounds obtained in relatively facile way with satisfactory (when regarding macrocyclization reactions) 24–55% yields. It makes above macrocycles promising potential metal cation complexing reagents in analytical chemistry providing that presenting satisfactory selectivity.

The structure of all new compounds was confirmed by spectroscopic methods: ^{1}H and ^{13}C NMR, HRMS and FTIR spectra (ESI Fig. S1-S16). The structure of macrocycles crystalizing in a form suitable for X-ray analysis was confirmed in a solid state. The structure of selected macrocycles was also investigated in solution using NMR spectroscopy (vide infra).

3.2. Description of X-ray structures

Compound **1** forms red, needle – like crystals with monoclinic symmetry. Structure of **1** was solved in the space group $P2_1/c$ and refined without any special treatment. Crystallographic details are listed in Table 1. The asymmetric unit contains one macrocyclic molecule. Atom labeling scheme is shown in Fig. 2.

Imidazolic N–H group is directed to the center of the macrocycle and does not form any hydrogen bonding in the crystalline state. The whole molecule is twisted, which manifests in a dihedral angle between the phenyl rings C4–C9 and C14–C19 equal to 20.2(2). The imidazole ring is almost coplanar with phenyl C14–C19, perhaps due to stacking interactions. Such an interaction with 3.858(2) Å inter-centroid distance is indeed formed between the imidazole ring and C14–C19 phenyl ring from a neighbour molecule, generated by inversion symmetry (1-*x*, 2-*y*,1-*z*).

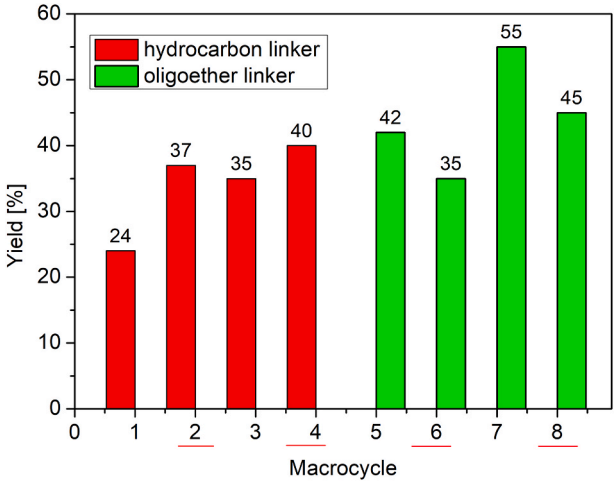

Fig. 1. The comparison of macrocyclization yield for compounds **1**–**8**. (No. of 4-methylimidazole derivatives are red underlined).

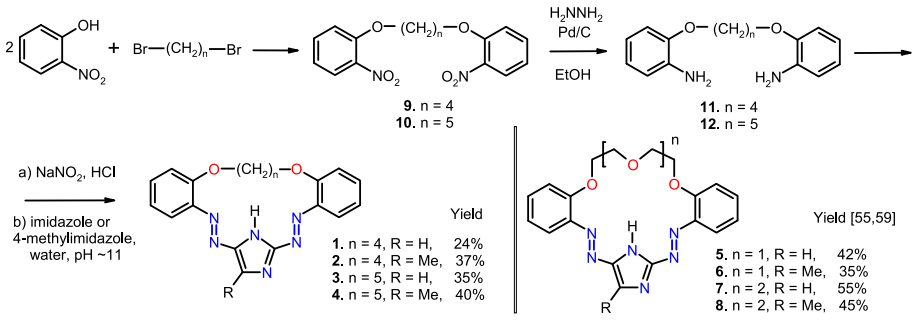

Scheme 1. Synthesis of macrocyclic compounds **1**–**4** with hydrocarbon linker and formulas of macrocycles bearing oligoether moiety **5**–**8**.

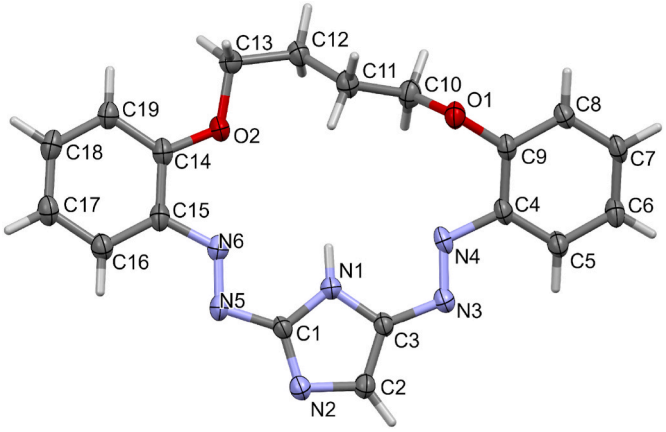

Fig. 2. Molecular view of **1**, showing atom labeling scheme. Displacement ellipsoids drawn at 50% probability level. Selected bond lengths (Å) and angles (°): N3–N4 1.267(4), N5–N6 1.268(4), N1–C1 1.347(5), N1–C3 1.360(5), N2–C1 1.323(5), N2–C2 1.381(5), C2–C3 1.373(5), N5–C1 1.408(5), N3–C3 1.392(5); valence angles: C9–O1–C10 116.1(3), C14–O2–C13 120.6(3), C1–N1–C3 106.5(3), C1–N2–C2 104.2(3), C3–C2–N2 109.7(3), N4–N3–C3 111.0(3), N3–N4–C4 114.9(3); torsions C8–C9–O1–C10 104.3(4), C9–O1–C10–C11 158.2(3), O1–C10–C11–C12 173.0(3), C10–C11–C12–C13 161.4(3), C11–C12–C13–O2 -62.6(4), C12–C13–O2–C14–179.3(3), C13–O2–C14–C19 13.6(6).

Compound **3** forms red crystals of needle habit. Its structure was solved and refined in the orthorhombic system, space group *Pnma* with four molecules in the unit cell. Structure **3** was refined making an assumption that the electron density in the mean unit cell has higher symmetry than actual molecules. The mean electron density is an average of the molecule and its mirror plane reflection. Thus, the asymmetric unit, being half of the molecule, contains N3–H3 and (C11–H11 and N4) and C9, H9A, H9B atoms with occupation factor equal to ½ (see Fig. 3). Dihedral angle between ring C1–C6 and its symmetry related counterpart (by mirror plane with symmcode: (x, 3/2 -y, z)) is equal to 43.20(4)°.

Structure of **4** was solved in the space group $P2_1/c$ and refined without any special treatment. The asymmetric unit contains one molecule and the unit cell four (Z = 4). Atom numbering scheme is shown in Fig. 4.

Again the imidazolic NH group is not engaged in hydrogen bonding. Bond lengths and valence angles are rather typical. The rings in the molecule are not coplanar. Dihedral angle between rings C5–C10 and C16–C21 equals to 26.72(12)°. Imidazole ring forms dihedral angles of 15.51(13)° with C5–C10 and 17.75(13)° with C16–C21 ring. Stacking interactions seems to play a secondary role in crystal packing due to large slippage of all the rings.

Compound **5** crystallizes in the space group *I2/m* (No. 12, cell choice 3 of *C2/m*). Cell parameters: (*a, b, c* (Å); *α, β, γ* (°) = 7.7187 (17), 31.861 (9), 29.749 (6); 90, 94.805 (17), 90). The structure was solved, but not refined to a satisfactory quality and therefore it was not deposited in the Cambridge Database. Raw results indicate the asymmetric unit contains one regular macrocycle molecule and two halves of the two other, chemically identical, macrocycles, both having mirror *m* symmetry. Each macrocyclic molecule is accompanied with a water molecule forming hydrogen bonding with an imidazole N-atom directed to the ring centre.

Compound **6** also forms red needle crystals. Structure of **6** was solved in the space group $P2_12_12_1$ and refined as the 2-component inversion twin (basf refined to meaningless −0.04537+-7.2). Atom labeling scheme is shown inFig. 5. Bond lengths and valence angles are not unusual. The imidazole N–H group is directed to the centre of the macrocycle but no hydrogen bonding is formed.

Etheric O2 atom is placed ca. 1 Å above the common molecular plane. The imidazole ring and C15–C20 phenyl ring are almost coplanar (1.7(7)°) and the other C5–C10 phenyl ring is only slightly twisted forming a dihedral angle equal to 11.2(7) ° to the imidazole ring. Stacking interactions play a marginal role in the crystal packing since the shortest ring inter-centroid distances are greater than 4 Å (based on PLATON results).

3.3. Structure in solution

The structure of 18-membered derivatives bearing 4-methylimidazole, namely compounds **4** and **6**, was investigated in solution using

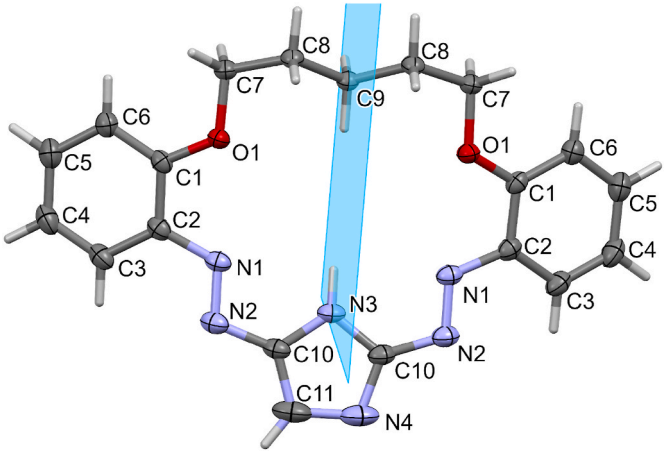

Fig. 3. Molecular view of **3** showing atom labeling scheme of the asymmetric unit and the molecule. Displacement ellipsoids drawn at 50% probability level. Atoms with repeated labels are related by the mirror symmetry (*x*, 3/2 - *y*, *z*). Selected bond lengths (Å) and angles (°): N1–N2 1.2700(14), O1–C1 1.3574 (13), O1–C7 1.4382(13), N1–C2 1.4031(16), N2–C10 1.3918(17), N3–C10 1.3627(14), N4–C10 1.3409(17), N4–C11 1.404(17); valence angles: C1–O1–C7 118.16(9), O1–C7–C8 106.93(9), N2–N1–C2 116.02(10), N1–N2–C10 109.86 (10), N3–C10–N2 123.99(10), N4–C10–N2 126.74(12), N4–C10–N3 109.14 (12); torsions C6–C1–O1–C7 -5.90(16), C1–O1–C7–C8 177.71(9), O1–C7–C8–C9 61.59(13), C7 C8 C9 C8#1 178.46(8).

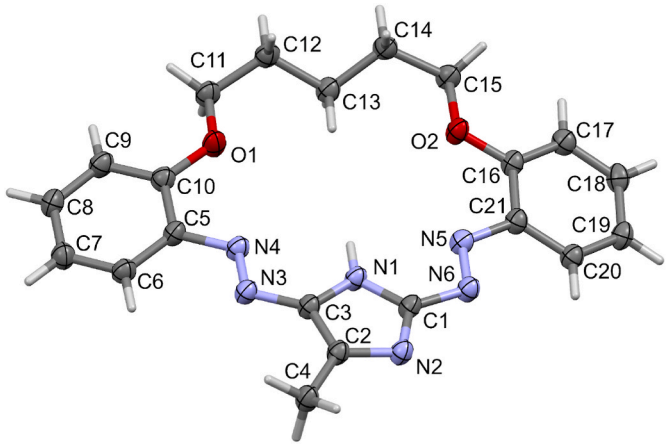

Fig. 4. Molecular view of **4** showing atom labeling scheme. Displacement ellipsoids drawn at 50% probability level. Selected bond lengths (Å) and angles (°): N3–N4 1.278(3), N5–N6 1.273(3), O1–C10 1.352(3), O1–C11 1.440(3), N1–C1 1.345(3), N1–C3 1.365(3), N2–C1 1.331(3), N2–C2 1.371(3), C2–C3 1.386(3), C2–C4 1.491(3), N3–C3 1.374(3), N4–C5 1.403(3); valence angles: C10–O1–C11 118.68(18), C16–O2–C15 117.78(16), C1–N1–C3 106.87(18), C1–N2–C2 104.58(18), N2–C1–N1 112.70(19), N2–C2–C3 109.84(19), N1–C3–C2 105.99(18); torsions: C5–C10–O1–C11 169.6(2), C10–O1–C11–C12 169.5(2), O1–C11–C12–C13 61.8(3), C11–C12–C13–C14 –175.1(2), C12–C13–C14–C15 –178.85(19), C13–C14–C15–O2 -60.5(3), C16–O2–C15–C14 –177.98(19).

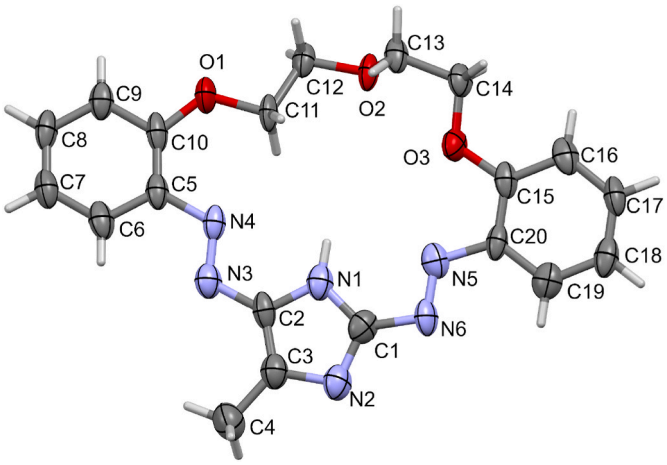

Fig. 5. Molecular view of **6** showing atom labeling scheme. Displacement ellipsoids drawn at 50% probability level. Selected bond lengths (Å) and angles (°): N3–N4 1.290(13), N5–N6 1.269(14), N1–C1 1.363(15), N1–C2 1.372(14), C2–C3 1.367(17), C3–C4 1.491(17), O1–C10 1.385(14), O1–C11 1.430(12), O2–C12 1.435(12), O2–C13 1.437(12); valence angles: C10–O1–C11 124.2 (10), C12–O2–C13 111.9(8), C15–O3–C14 119.5(8), N2–C1–N1 112.2(11), C1–N2–C3 104.5(10), C2–C3–N2 109.4(11), C3–C2–N1 107.8(11), C1–N1–C2 106.0(11); torsions: C5–C10–O1–C11 –2.4(19), C10–O1–C11–C12n 175.6(9), O1–C11–C12–O2 -178.6(8), C11–C12–O2–C13 –85.4(11), C12–O2–C13–C14 169.2(10), O2–C13–C14–O3 -69.1(12), C13–C14–O3–C15 –175.5(9), C14–O3–C15–C16 –4.4(16).

NMR spectroscopy to find out if the linker type affects the position of N–H imidazole proton. The ROESY spectrum of the **4** clearly indicates that the aromatic proton is bound to the nitrogen N1(cf. crystal structure Fig. 6) of imidazole, setting the N–H proton inside the molecule's macrocyclic ring. The proton exhibits the ROE effect to the methylene group of the aliphatic chain. If the proton was bound to the second imidazole nitrogen (N2), then a strong cross-space correlation to the methyl group should be observed in the ROESY spectrum.

The ROESY spectrum of **6** (Fig. S16a) does not show diagnostic effects, which could define the position of the aromatic N–H proton. Only on the basis of the lack of interaction with the methyl group can it be suggested that the discussed proton is also bound to the same nitrogen of imidazole ring, like in the case **4**.

3.4. Lipophilicity

The lipophilicity of newly obtained compounds **1**–**4** and oligoether analogs **5**–**8** with imidazole and 4-methylimidazole residues were determined to link this parameter with their chromoionophoric properties when studied in solution and incorporated in the receptor layer. The lipophilicity of these compounds has not been determined before. The lipophilicity ($logP_{TLC}$) parameters determined using reverse phase thin layer chromatography method [48,60,66] for macrocycles **1**–**8** are presented in Fig. 7 and collected in Table S1.

As expected, the $logP_{TLC}$ values obtained for compounds (**1**–**4**) with a hydrocarbon chain are greater than those received for macrocyles (**5**–**8**) with an oligoether linkage. However, the exception is compound **6**, which, despite having a shorter chain, has a higher lipophilicity value than the rest of the oxygen analogs. In addition, the type of substituent in the imidazole structure also affects the $logP_{TLC}$ value - 4-methylimidazole derivatives are more lipophilic than macrocyles (**1**, **3**, **5** and **7**) bearing unsubstituted imidazole.

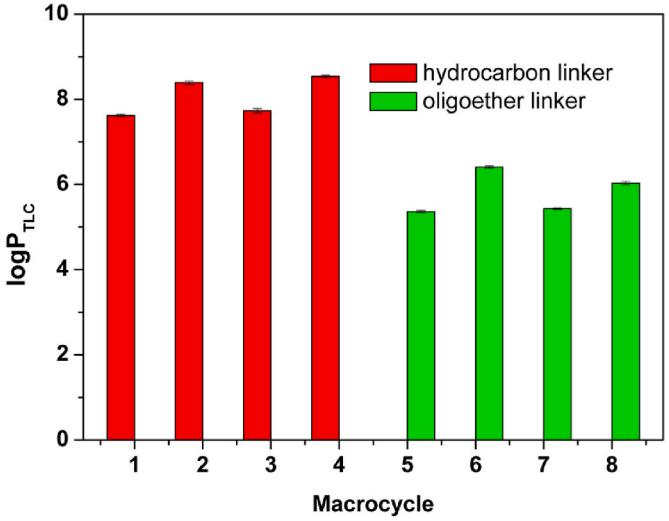

Fig. 7. Comparison of lipophilicity parameter ($logP_{TLC}$) for macrocycles **1**–**8**.

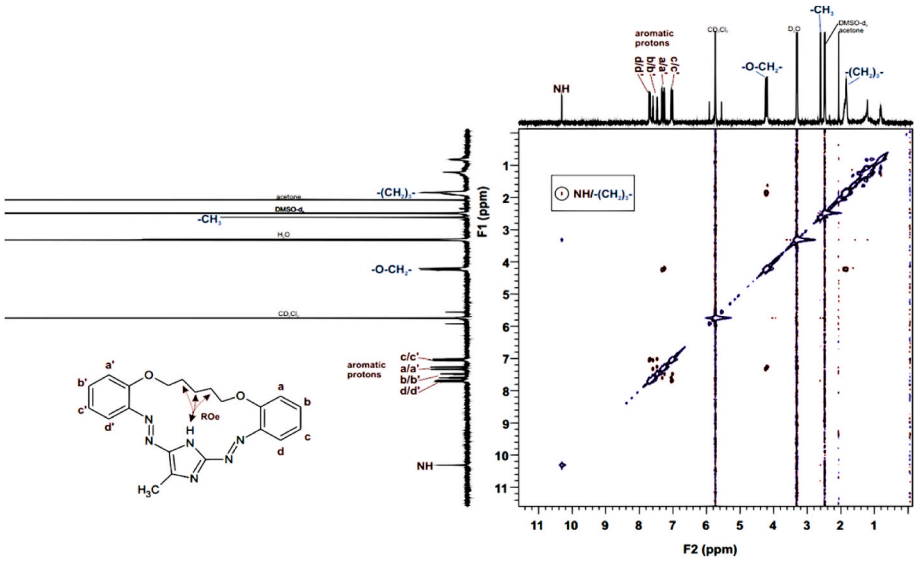

Fig. 6. ROESY spectrum of **4** in DMSO-d_6.

3.5. Acid base-properties of novel macrocycles 1-4

Color properties of macrocyclic compound **1**–**8** are affected by the presence of the methyl group in the imidazole ring. In general 4-methylimidazole derivatives have deeper colors both in acetonitrile and its mixture with water.

The acid-base properties of the newly obtained compounds **1**–**4** were tested in acetonitrile and in a mixture of acetonitrile:water (9:1, v/v). In all cases, more or less intense changes in the color of solutions are observable, both in the presence of *p*-toluenesulfonic acid (TsOH) and tetra-*n*-butylammonium hydroxide (TBAOH) (Fig. S17). In the case of compounds **2**–**4**, the addition of water to acetonitrile causes a partial or complete color withdrawal to the color corresponding to macrocyclic compounds in acetonitrile. Only for compound **1** a color change from orange to yellow is maintained in the presence of *p*-toluenesulfonic acid in a solution of acetonitrile:water 9:1 (v/v). Color changes caused by the pH alteration are relatively more distinct for oligoether bearing macrocycles **5**–**8**. The observed color changes can be explained by the course of absorption spectra registered in the presence of *p*-toluenesulfonic acid. It is exemplified by absorption spectra registered for spectrophotometric titration of compounds **1**–**4** with TsOH in acetonitrile (Fig. S18). The presence of acid is manifested by the increase of the intensity of the absorption bands below 450 nm. The main absorption band corresponding to protonated form is slightly red shifted, however it largely overlaps the main absorption band. In Fig. S19 spectral changes upon titration of compounds **1**–**4** with TBAOH in acetonitrile are presented. Bands corresponding to deprotonated forms of macrocycles are observed at ~510 nm (for **1** and **3**) and ~540 nm (for **2** and **4**). It explains more significant color changes of solutions from orange to purple of compounds **2** and **4** and only a deepening of the color in the case of solutions of compounds **1** and **3**. In Table S2 UV–Vis spectral characterization of compounds **1**–**4** in acetonitrile is presented.

Color properties of macrocyclic compound **1**–**8** are affected by the presence of the methyl group in the imidazole ring. In general 4-methylimidazole derivatives have deeper colors both in acetonitrile and its mixture with water than imidazole bearing macrocycles. When comparing the position of the longwave absorption maximum (Fig. 8) in acetonitrile for 4-methylimidazole derivatives and imidazole ones it is well seen that the last absorbs at lower wavelengths. Comparing the position of absorption bands it can be concluded that excitation energy for 4-methylimidazole derivatives is lower. The electronic effect of the methyl group can contribute to this phenomena. However one of the factors which affect the absorption of light is geometry of the molecule. If a molecule is planar then the energy of excitation is lower and as a result the absorption maximum is bathochromically shifted when comparing molecules of similar type, but of disordered planarity. This can find confirmation in comparison of crystal structures of molecules **3** and **4** (having in mind that the direct comparison cannot be done, because of the different chemical environment of the molecule in a solid state and in solution). Molecule of compound **4** is more planar than the molecule of macrocycle **3**. And probably thus 4-metyhlimidazole macrocyclic azoderivatives have deeper colors.

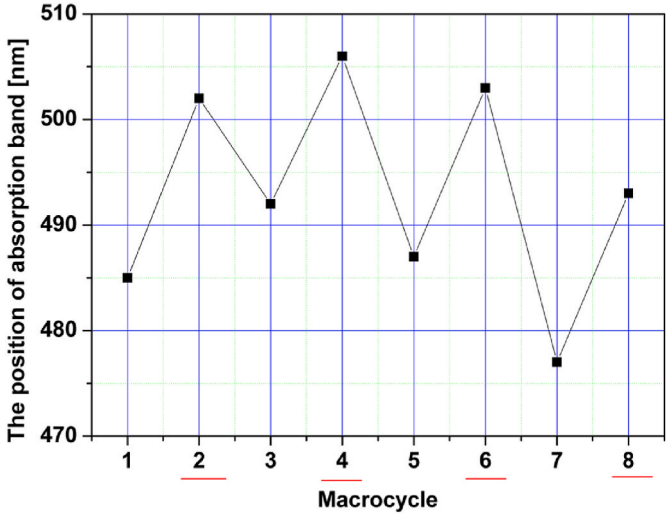

Fig. 8. Comparison of the position of the longwave absorption bands of macrocycles **1**–**4** in acetonitrile (No. of 4-methylimidazole derivatives are red underlined).

3.6. Metal cation complexation of in solution

The first step of the study of chromoionophic properties of compounds **1**–**8** included the investigation of color changes of solutions in the presence of metal salts. In Fig. S20 color of the solutions of compounds **1**–**4** (qualitative tests carried out as an addition to the solution of the macrocyclic compound of excess salt in solid form) in the presence of alkali and alkaline earth metal perchlorates. The presence of the above metal perchlorates has no significant effect on the color of solutions of compounds **1**–**4** with hydrocarbon linker in acetonitrile and acetonitrile: water (9:1, v/v) solvent system. On the other hand, the color of solutions of oligoether derivatives **5**–**8** is affected by the presence of alkali and alkaline earth metal perchlorates. Color changes from orange to yellow. The different affinity of compounds **1**–**4** and **5**–**8** to alkali and alkaline earth metal cations can be explained on the basis of the hard and soft acid and bases theory. Alkali and alkaline earth metal cations are hard acids interacting with hard bases. Oxygen atoms act as hard donor centers in oligoether moiety. Macrocycles **5**–**8** are richer in coordination oxygen atoms, thus their affinity towards hard metal cations is higher. The presence of water - acting as a competitive ligand - causes a partial or complete return to the color corresponding to the original color of the macrocycle solution, which is an effect of high hydratation energies of alkali and alkaline earth metal cations in water.

Besides oxygen coordination centers in investigated macrocycles nitrogen atom(s) of azo group(s) and imidazole residue can also serve as donor atoms in metal complexation. Nitrogen is softer than oxygen donor thus the complex formation with softer metal cation can be obviously expected. The results of quantitative tests for selected heavy metal perchlorates are presented in Fig. 9. The presence of heavy metal perchlorates affects the color of solutions of both groups of investigated macrocycles: hydrocarbon **1**–**4** and oligoether linked **5**–**8**. Solutions of **1**–**4** change color from orange/red to red/purple in the presence of lead (II) perchlorate. The presence of water causes an increase of color intensity in the presence of copper(II) and lead(II) perchlorates and a color withdrawal to the initial color of the solution in the presence of zinc(II) and cadmium(II) ions. The exception is the solution of **1**, for which color changes from orange to yellow in the presence of cadmium(II) in acetonitrile and its mixture with water. Unfortunately this selective color change is observable only when a high excess of cadmium(II) perchlorate is used. This limits the potential applications of macrocycle **1** as cadmium selective probe in real e.g. environmental samples.

Among oligoether derivatives **5**–**8** a solution of **5** shows the less distinct color changes caused by the presence of heavy metal perchlorates. Only a slight color change is observed in the presence of zinc(II) and lead(II) perchlorates in acetonitrile:water mixture (9:1, v/v). The solutions of compounds **6** and **8** change color from orange to purple in the presence of copper(II) and lead(II) perchlorates in acetonitrile and for **6** color change is still observable in water containing the solvent system. Solution of compound **7** changes color in the presence of copper (II) salt from orange to red in acetonitrile and to purple in a mixture of acetonitrile:water (9:1, v/v). In the mixture with water, a change in color is observed in the presence of nickel(II) and zinc(II) perchlorates for solutions of compounds **7** and **8**.

On the basis of the qualitative research, it can be assumed that the compounds **1**–**4** with a hydrocarbon chain present promising heavy

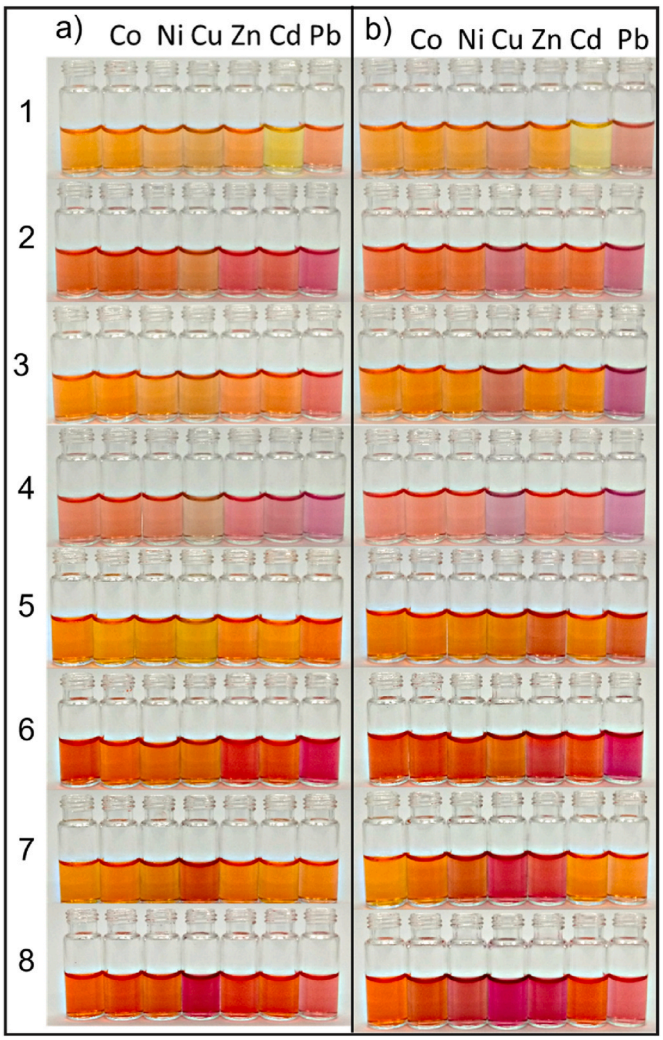

Fig. 9. Color changes of macrocyclic compounds **1**–**8** in the presence of selected heavy metal perchlorates in a) acetonitrile and b) acetonitrile:water (9:1,v/v) solutions.

metal receptors in water containing solvent system. The greater selectivity towards heavy metal ions compared to oligoether analogs **5**–**8** can be explained by the reduction in the number of hard coordination centers in the molecule.

3.6.1. *Lead(II) complexes*

Observing the color changes in qualitative tests for macrocycles **1**–**8** heavy metal cation complexation was investigated by UV–Vis absorption spectrophotometry in acetonitrile and acetonitrile:water (9:1, v/v) solvent system. Changes in the absorption spectra of solutions of compounds **1**–**4** and **5**–**8** during titration with lead(II) perchlorate in acetonitrile are shown in Fig. S21 and Fig. S22 respectively. Complex formation with lead(II) is connected with formation of a new absorption band. However, absorption bands of macrocycles and their complexes are poorly separated, thus only a slight change in color upon complexation is observable. Spectral changes are more distinct for **1**–**4** than for **5**–**8** titration experiments. In a mixed solvent system - acetonitrile:water (9:1, v/v) – band separation for **3** and **4** and their complexes is ca. 50 nm (Fig. 10). In case of compounds **1** and **2** upon spectrophotometric titration a wide band of the complex is formed in the range of 530–650 nm and 560–690 nm, respectively.

Spectral changes upon UV–Vis titration of **5**–**8** with lead(II) perchlorate in acetonitrile:water (9:1, v/v) are shown in Fig. 11. Spectral shift between the absorption band of macrocycle and its complex with lead(II) is ca. 50 nm for **5** and **6**. Complex band is well pronounced. For **7** and **8** spectral shifts are also observed, however the complex absorption bands are less developed.

On the basis of Job's plots [71], it can be concluded that complex of 3:2 (ligand:cation) stoichiometry is formed in the systems **1**-Pb(II), **2**-Pb (II), **3**-Pb(II) and **4**-Pb(II), both in acetonitrile and in the mixture with water (Fig. S23 and Fig. S24, respectively). Stoichiometry of 3:2 (crown: Pb(II)) in acetonitrile was earlier confirmed for pyrrole bearing macrocycles [60], so a similar mode, namely triple-decker sandwich type complex, can be also proposed for imidazole derivatives. Stability constant values (logK) of the complexes of **1**–**8** with lead(II), calculated from titration data using the OPIUM program [67] are presented in Fig. 12 and summarized in Table S3.

In acetonitrile, the highest values of stability constant (logK) have lead(II) complexes of 21-membered crowns **7**–**8**, 19.66 ± 0.10 and 20.16 ± 0.12, respectively. Macrocycles of 17- and 18-membered rings form complexes of lower and comparable values of stability constants (log K ~18), independent of the type of linker (hydrocarbon/oligoether). However, the lowest value, 17.24 was found for the lead(II) complex of macrocycle **5**. The value of the stability constant of lead(II) complexes is influenced by the size of the macroring, which defines the size of the molecular cavity. 21-membered crowns form stronger complexes with lead(II) than 17- and-18 membered macrocycles. Similar trend in stability constant values was found for pyrrole bearing macrocycles [60]. Moreover, lead(II) complexes formed by macrocyclic compounds bearing 4-methylimidazole residue (**2**, **4**, **6** and **8**) are characterized by higher values of stability constants compared to their imidazole analogs. It can be another confirmation of the effect of the methyl substituent in heterocyclic ring on the geometry of the molecule. When a molecule is more planar the accessibility of binding sites is better and ion is bound more efficiently. The trend of stability constant values of lead(II) complexes is similar in acetonitrile:water (9:1,v/v). Not surprisingly in mixed solvent system stability constant values are lower than in acetonitrile.

3.6.2. *Copper(II) recognition in solution*

Due to color changes observed during qualitative tests in the presence of copper(II) perchlorate, for compounds **1**–**4** spectroscopic titration with copper(II) perchlorate was carried out in acetonitrile and the mixture of this solvent with water (Fig. S25 and Fig. S26). The registered spectra are characterized with an increase of band intensity in the 310–450 nm wavelength range and the formation of a broad bathochromically shifted band $\lambda = 550–650$ nm. The changes, similar to the spectral changes observed in the presence of TsOH, are not spectacular. On the basis of titration experiments the determination of a reliable value of stability constant for copper(II) complexes was not possible.

3.7. *Metal ion recognition in receptor layers*

3.7.1. *Preliminary studies*

Macrocycles **1**–**8** were tested as lead(II) and copper(II) receptors upon immobilization in a solid matrix. For current studies porous glass (PG-PS) was used. In preliminary studies the content of chromoionophore in solid material was established as 0.5 mg per g of porous glass.

Materials with compounds **1** and **2** have shown no color change in the presence of copper(II) and lead(II) nitrates. In Fig. 13 color changes (photos were taken using Smartphone camera) of sensors with chromoionophores **3**–**8** after contact with solutions of different concentrations of copper(II) or lead(II) nitrate are presented. Observable color changes, which can be traced by "the naked eye" were found to more or less degree for all sensors. However, in the case of materials with chromoionophores **4**, **6** and **8** the observed color changes were more distinct than for sensors with compounds **3**, **5** and **7**. Color changes were from the orange/red to violet/blue depending on the macrocycle and the metal nitrate. More significant color change was observed for lead(II) nitrate then for copper(II).

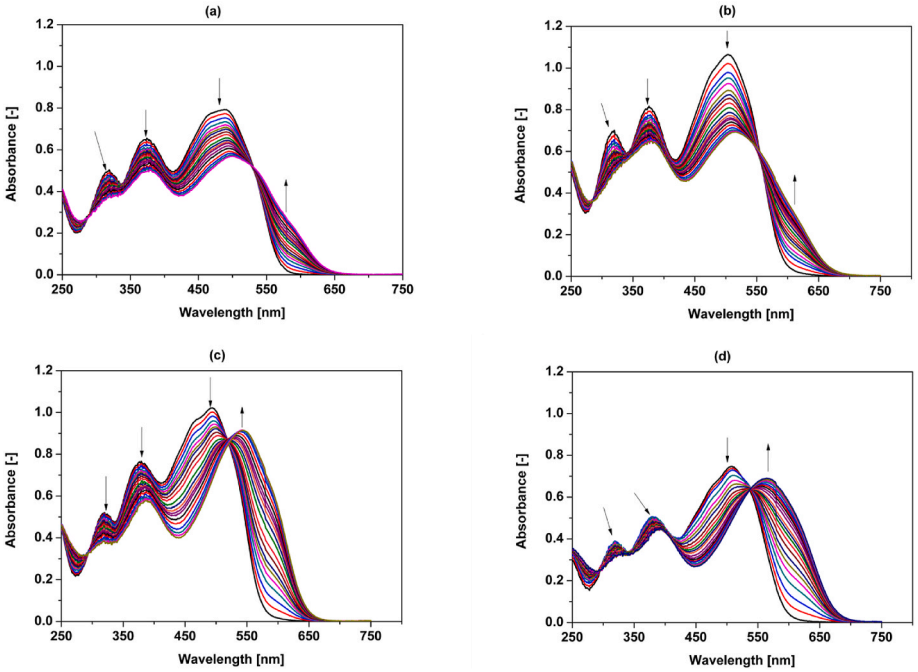

Fig. 10. Changes in absorption spectra of **1**–**4** during spectrophotometric titration with lead(II) perchlorate in acetonitrile:water (9:1, v/v) mixture: a) **1** ($c_1 = 4.97 \times 10^{-5}$ M) ($c_{Pb} = 0$–6.97×10^{-5} M); b) **2** ($c_2 = 4.96 \times 10^{-5}$ M) ($c_{Pb} = 0$–8.03×10^{-5} M); c) **3** ($c_3 = 5.09 \times 10^{-5}$ M) ($c_{Pb} = 0$–1.97×10^{-4} M); d) **4** ($c_4 = 4.91 \times 10^{-5}$ M) ($c_{Pb} = 0$–2.43×10^{-4} M).

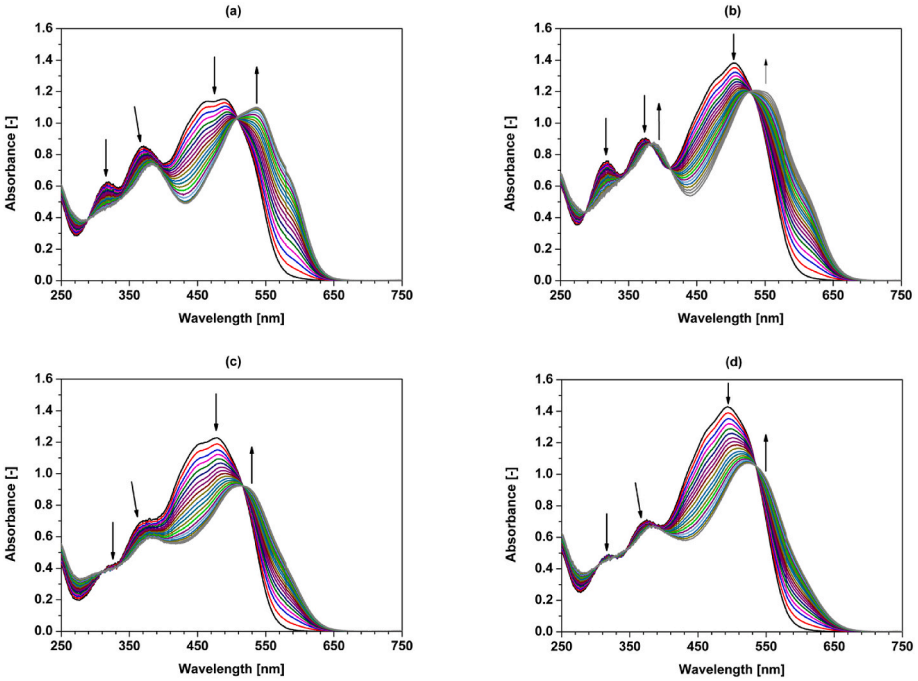

Fig. 11. Changes in absorption spectra of **5**–**8** during spectrophotometric titration with lead(II) perchlorate in acetonitrile:water (9:1, v/v) mixture: a) **5** ($c_5 = 4.97 \times 10^{-5}$ M) ($c_{Pb} = 0$–7.11×10^{-5} M); b) **6** ($c_6 = 4.99 \times 10^{-5}$ M) ($c_{Pb} = 0$–7.58×10^{-5} M); c) **7** ($c_7 = 4.90 \times 10^{-5}$ M) ($c_{Pb} = 0$–9.46×10^{-5} M); d) **8** ($c_8 = 5.00 \times 10^{-5}$ M) ($c_{Pb} = 0$–8.52×10^{-5} M).

3.7.2. PG-PS sensor layers – the effect of amount of chromoionophore

The amount of chromoionophore can affect the color response towards analytes. Thus to optimize the amount of chromoionophore, sensor materials with different quantities (0.25, 0.50, 0.75 and 1.00 mg/g) of macrocycles **3**–**8** were prepared. The color response towards the presence of copper(II) and lead(II) nitrates is shown in Fig. 14 taking the material with immobilized macrocycle **6** as an example. The lowest amount of chromoionophore, namely 0.25 mg/g, seems to be not sufficient to observe significant color changes. This can be an effect of the insufficient amount of chromoionophore for complex formation. On the other hand, the use of higher amounts, 0.75 and 1.00 mg/g, results in material which gives no color change - red sensor material changes the hue of the color in the presence of copper(II) and lead(II) nitrates. The higher concentration of chromoionophore can affect its organization in

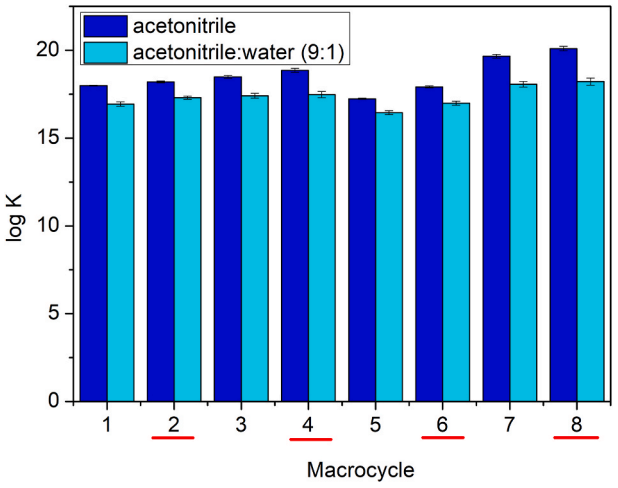

Fig. 12. Comparison of stability constants (logK) of 3:2 (crown:Pb(II)) complexes of macrocycles **1**–**8** (4-methylimidazole derivatives are red underlined) in acetonitrile and acetonitrile:water (9:1, v/v) solvent system.

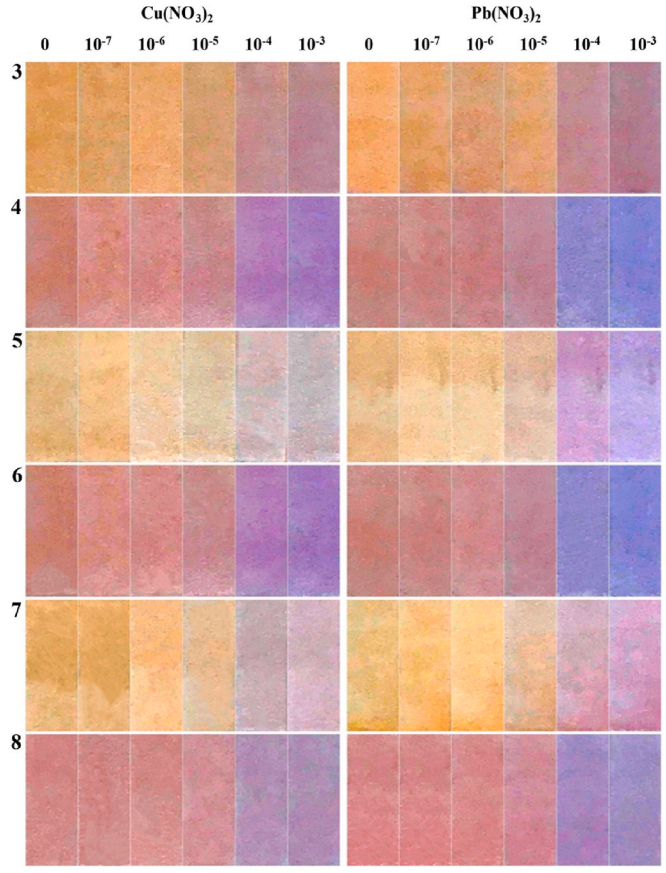

Fig. 13. Color changes of sensor layers with compounds **3**–**8** (0.5 mg/g) in solutions of different concentrations [M] of copper(II) or lead(II) nitrate.

solid material which makes complex formation not fully effective. On the basis of above, the amount of 0.5 mg/g seems to be optimal when considering the color response of sensing material. Thus materials containing this amount of chromoionophores were used in further studies.

3.7.3. Response time

Response time is one of the important factors when considering the

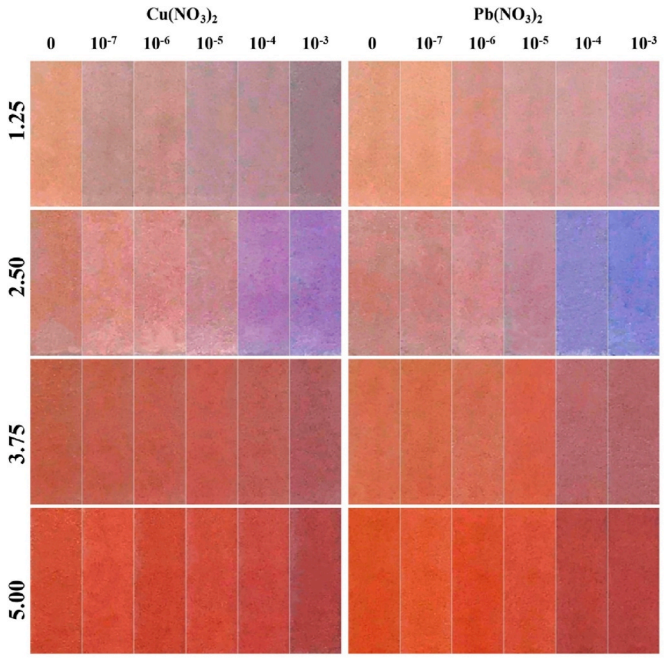

Fig. 14. Color changes of sensor layers with compound **6** - used in different amounts (mg/g) - after contact with solutions of different concentrations [M] of copper(II) or lead(II) nitrates.

applicability of receptor layers as sensor material. To determine the response time, experiments where sensor layers were immersed in solution copper(II) of lead(II) nitrate (10^{-4} M or 10^{-5} M) with contact time up to 10 min were carried out. As a response, the change of the ΔE_{RGB} parameter as a function of time needed for constant optical signal setting up was taken. The sensors were found to reach 95% of the final signal (t_{95}) within 3 min for materials with compound **3**–**6** and 4 min for with macrocyles **7** and **8** (Fig. 15)

3.7.4. Interfering ions

The response of prepared sensor layers towards copper(II)/lead(II) was investigated in the presence of several interfering metal nitrates: sodium, potassium, calcium, magnesium, strontium, barium, nickel(II), copper(II), zinc(II) and lead(II) at fixed pH 6. In Fig. 16 the influence of addition of 10-fold molar excess of interfering ion salt on the color change ΔE_{RGB} of sensor material immersed in 10^{-4} M solution of copper (II) or lead(II) nitrate is shown. From Fig. 16 it can be concluded that during the detection/determination of lead(II), significant color changes are observed for copper(II), and when copper(II) is the main analyte, lead(II) must be considered as the most interfering cation.

3.7.5. Linear response

Linear response range, defined as the change of ΔE_{RGB} vs. copper(II) or lead(II) concentration was determined for sensor layers with macrocycles **3**–**8**. In Fig. S27 the dependence of color change (ΔE_{RGB}) vs. concentration of copper(II) for materials with compounds **3**–**8** is shown. The linear response of sensor layers (Table S4) with compounds **4**–**8** toward copper(II) are in range 1.0×10^{-6} – 1.0×10^{-3} M, only for sensor with chromoionophore **3** have narrower range 1.0×10^{-5} – 1.0×10^{-3} M. The lowest LOD 4.09×10^{-7} M was obtained for a sensor with compound **7**.

All linear response ranges for lead(II) for materials with macrocycles **3**–**8** are collected in Table S5 and curves are shown in Fig. S28. The narrower range of linear response 1.0×10^{-5} – 1.0×10^{-3} M was obtained for sensor material with compound **3**. The rest of investigated materials are characterized by a linear response range within 1.0×10^{-6} – 1.0×10^{-3} M with the lowest LOD = 2.84×10^{-7} M for optical sensor

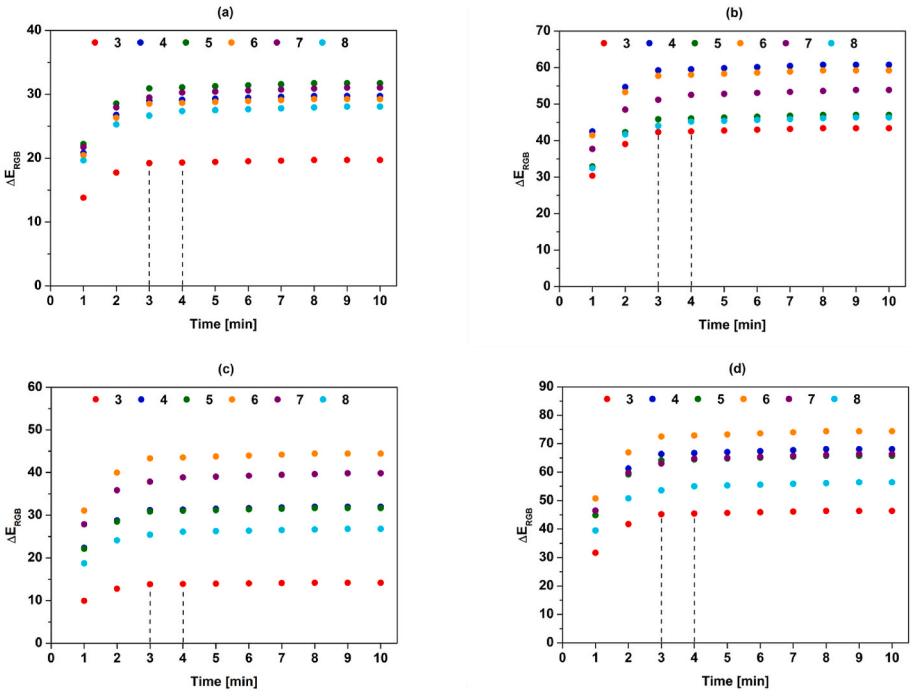

Fig. 15. The color change (ΔE_{RGB}) of sensor layers with chromoionophores **3**–**8** upon immersion in metal nitrates: a) copper(II) 10^{-4} M, b) copper(II) 10^{-5} M, c) lead (II) 10^{-4} M and d) lead(II) 10^{-5} M over time.

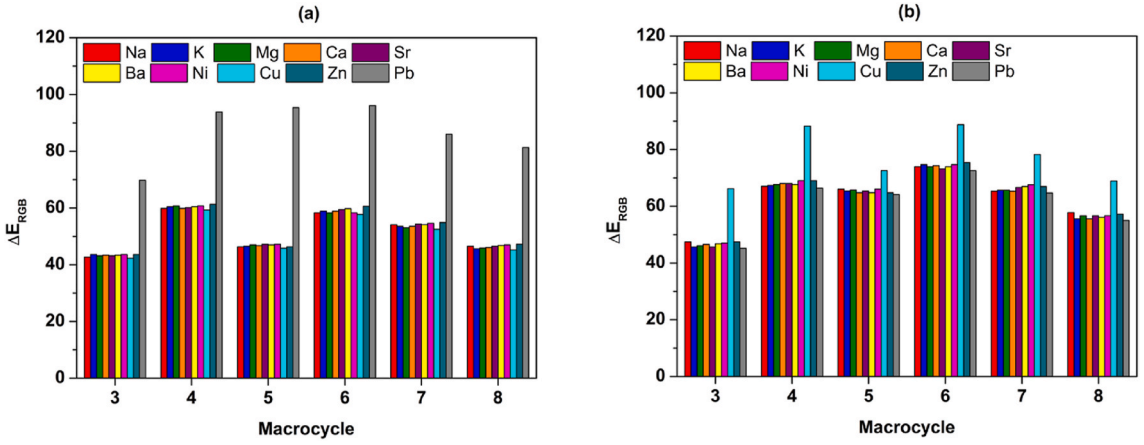

Fig. 16. Interferences of several metal cations (used in 10-fold molar excess), to color change (ΔE_{RGB}) of sensing layers with chromoionophores (0.5 mg/g) **3**–**8** towards: a) copper(II) and b) lead(II) nitrate at pH 6.

containing crown **6**.

The weaker point of the proposed optical sensors is their inability to be regenerated. While the color of the sensor used to detect copper(II) or lead(II) returns to its original color after immersion in an acid solution (0.1 M nitric acid), repeated placement in a salt solution does not generate a color change. Therefore, these sensors should be considered as single-use materials.

3.7.6. *Applications for real samples analysis*

The possibility of application of the proposed sensor layers was assessed on three samples of spiked tap water from different regions of northern Poland. All measurements were done at pH 6.0. Comparison of the recovery results obtained for materials with chromoionophores **3**–**8** upon immersion of the sensor layer in samples with added copper(II) solution of different concentrations is collected in Table S6. The recoveries are at least about 97.13–104.40% (n = 3) for colorimetric detection (ΔE_{RGB}) for copper(II) concentrations in range from 1.0×10^{-6} M to 1.0×10^{-4} M. Analogous tests were carried out for lead(II) at the same concentration range. In this case recoveries were within 97.81–103.95% (n = 3) – Table S7.

3.7.7. *Comparison with the other reported sensing materials*

In Table 2 the properties of selected lead(II) and copper(II) selective sensing materials obtained in recent years and described in literature are listed for comparison with the materials obtained in this work.

From Table 2 it can be concluded that materials based on commercial porous glass obtained by us have more or less comparable properties to solutions described in literature. In comparison with other sensors which are based on silica materials, which use mostly covalently bonded sensing molecules, the main advantage of proposed materials is their facile preparation. Compared with classical optodes the proposed materials are prepared with a limited number of components. Thus the usage of chemicals in such an approach is minimized. The application of colorimetric detection with widely used mobile devices makes the

Table 2
Comparison of obtained sensing materials with already existing ones.

Copper (II) sensing materials						
Chromoionophore	Support	Method	Response time [min]	Linear response [M]	LOD [M]	Reference
HIBIN[a]	Sol-gel	Absorbance	2	$9.1 \times 10^{-8} - 1.1 \times 10^{-5}$	1.8×10^{-8}	[72]
Schiff base	Sol-gel	Absorbance	2	$8.5 \times 10^{-8} - 1.0 \times 10^{-5}$	1.5×10^{-8}	[73]
HQDB[b]	Hybrid Monolith	Absorbance	2	$4.7 \times 10^{-9} - 1.6 \times 10^{-6}$	7.1×10^{-9}	[74]
TPDP[c]	Mesoporous Silica	Absorbance	60–300	$3.2 \times 10^{-8} - 1.6 \times 10^{-6}$	4.4×10^{-9}	[75]
Hydroxyazocompound	CTA	Absorbance	3	$5.4 \times 10^{-8} - 2.5 \times 10^{-5}$	7.2×10^{-8}	[48]
		Colorimetric		$4.3 \times 10^{-7} - 2.5 \times 10^{-5}$	4.1×10^{-7}	
7	PG-PS	Colorimetric	4	$1.0 \times 10^{-6} - 1.0 \times 10^{-3}$	4.1×10^{-7}	This work
Lead(II) sensing materials						
Chromoionophore	Support	Method	Response time [min]	Linear response [M]	LOD [M]	Reference
DPDB[d]	Mesoporous Silica	Absorbance	40–180	$1.5 \times 10^{-11} - 7.8 \times 10^{-7}$	8.7×10^{-10}	[76]
DPAP[e]	Mesoporous Silica	Absorbance	5–15	$2.4 \times 10^{-8} - 9.7 \times 10^{-7}$	5.0×10^{-9}	[77]
Dithizone	Chitosan-Silica	Absorbance	3	$9.7 \times 10^{-7} - 5.3 \times 10^{-6}$	5.3×10^{-7}	[78]
HMBA[f]	Silica Monolith	Absorbance	30–180	$9.7 \times 10^{-12} - 7.8 \times 10^{-7}$	2.0×10^{-9}	[79]
Diazocrown	CTA	Absorbance	7	$8.1 \times 10^{-8} - 2.2 \times 10^{-5}$	1.2×10^{-8}	[61]
		Colorimetric		$7.8 \times 10^{-7} - 2.1 \times 10^{-4}$	8.6×10^{-7}	
6	PG-PS	Colorimetric	3	$1.0 \times 10^{-6} - 1.0 \times 10^{-3}$	2.8×10^{-7}	This work

[a] N′-(2-hydroxy-5-iodobenzylidene)isonicotinohydrazide
[b] 4-hexyl-6-(quinolin-8-yldiazenyl)benzene-1,3-diol.
[c] 4-*tert*-octyl-4-((phenyl)diazenyl)phenol.
[d] 4-dodecyl-6-((4-(hexyloxy)phenyl)diazenyl)benzene-1,3-diol.
[e] 4-dodecyl-6-(2-pyridylazo)-phenol.
[f] 6-((2-(2-hydroxy-1-naphthoyl)hydrazono)methyl)benzoic acid.

sophisticated measurement equipment almost no needed.

4. Conclusions

New chromogenic macrocycles containing a hydrocarbon linker and imidazole or 4-methylimidazole were obtained. Synthetic protocol enables the preparation of the macrocycles with satisfactory yields. The properties of the newly obtained macrocycles were compared with macrocycles linked via an oligoether bond. The effect of the type of heterocyclic residue and the type of linker is seen in color properties (deeper colors of 4-methylimidazole derivatives) and in metal cation affinity. The last is affected by the chemical environment, namely acetonitrile or acetonitrile:water mixture or hydrophilic solid support – porous glass. After physical immobilization of the macrocycles on porous glass, a selective color change was observed as an analytical response to the presence of heavy metal cations, namely lead(II) and copper(II). Promising properties, among investigated materials, have sensors based on crowns with oligoether moiety. Among them are an 18-membered crown with 4-methylimidazole (**6**) as lead(II) and 21-membered crown (**7**) with imidazole residue as copper(II) chromoionophore.

The optical sensors obtained by us, compared to many solutions proposed in the literature, are materials with an extremely simple composition: only chromophore and porous glass - which is one of the advantages of the proposed solution. And in conjunction with the fact that macrocyclic chromoionophores are relatively easy to prepare, our proposed approach, although imperfect, seems promising for further research and development of optical sensors. Another possible application of the proposed system, which is out of scope of this article, is the possibility of usage of the materials for detection and capturing of heavy metals from wastewater.

CRediT authorship contribution statement

Błażej Galiński: Conceptualization, Data curation, Formal analysis, Investigation, Methodology, Validation, Visualization, Writing – original draft, Writing – review & editing. **Jarosław Chojnacki:** Data curation, Investigation, Methodology, Visualization, Writing – original draft, Writing – review & editing. **Katarzyna Szwarc-Karabyka:** Data curation, Investigation, Writing – original draft. **Adrian Małkowski:** Data curation, Investigation. **Diana Sopel:** Data curation, Investigation. **Agnieszka Zwolińska:** Data curation, Investigation. **Ewa Wagner-Wysiecka:** Conceptualization, Data curation, Supervision, Validation, Visualization, Writing – original draft, Writing – review & editing.

Declaration of competing interest

The authors declare that they have no known competing financial interests or personal relationships that could have appeared to influence the work reported in this paper.

Data availability

Data will be made available on request.

Acknowledgments

This work was supported by the Faculty of Chemistry, Gdańsk University of Technology, No. 035376 and 036276 — internal grants from statutory funds. The financial support to maintenance of research facilities used in these studies from Gdańsk University of Technology by the DEC-2/2021/IDUB/V.6/Si grant under the SILICIUM SUPPORTING CORE R&D FACILITIES – "Excellence Initiative - Research University" program is gratefully acknowledged.

Appendix A. Supplementary data

Supplementary data to this article can be found online at https://doi.org/10.1016/j.dyepig.2023.111610.

References

[1] Tchounwou PB, Yedjou CG, Patlolla AK, Sutton DJ. Heavy metal toxicity and the environment. In: Luch A, editor. Molecular, Clinical and Environmental Toxicology, 101. Basel: Springer; 2012. p. 133–64. https://doi.org/10.1007/978-3-7643-8340-4_6.
[2] Rehman M, Liu L, Wang Q, Saleem MH, Bashir S, Ullah S, Peng D. Copper environmental toxicology, recent advances, and future outlook: a review. Environ Sci Pollut Res 2019;26:18003–16. https://doi.org/10.1007/s11356-019-05073-6.

[3] Buzea C, Pacheco I. Heavy metals: definition, toxicity, and uptake in plants. In: Faisal M, Saquib Q, Alatar AA, Al-Khedhairy AA, editors. Cellular and molecular Phytotoxicity of heavy metals, Nanotechnology in the life Sciences. Cham: Springer; 2020. https://doi.org/10.1007/978-3-030-45975-8_1.

[4] Belabed BE, Meddour A, Samraoui B, Chenchouni H. Modeling seasonal and spatial contamination of surface waters and upper sediments with trace metal elements across industrialized urban areas of the Seybouse watershed in North Africa. Environ Monit Assess 2017;189. https://doi.org/10.1007/s10661-017-5968-5.

[5] Gan Y, Huang X, Li S, Liu N, Li YC, Freidenreich A, Wang W, Wang R, Dai J. Source quantification and potential risk of mercury, cadmium, arsenic, lead, and chromium in farmland soils of Yellow River Delta. J Clean Prod 2019;221:98–107. https://doi.org/10.1016/j.jclepro.2019.02.157.

[6] Peng H, Chen Y, Weng L, Ma J, Ma Y, Li Y, Islam MS. Comparisons of heavy metal input inventory in agricultural soils in north and south China: a review. Sci Total Environ 2019;660:776–86. https://doi.org/10.1016/j.scitotenv.2019.01.066.

[7] Nassiri O, Rhoujjati A, Moreno-Jimenez E, Hachimi MLEL. Environmental and geochemical characteristics of heavy metals in soils around the former mining area of Zeïda (High Moulouya, Morocco). Water Air Soil Pollut 2023;234. https://doi.org/10.1007/s11270-023-06103-3.

[8] Kannan G, Roy PD, Sundar S, Usha T, Gowranppan M, Kishore PV, Periyasamy R, Johnatan MP, Chokkalingam L. Pollution assessment with respect to five heavy metals in urban soils of the Greater Chennai Region, Southeast Coast of India. Water Air Soil Pollut 2023;234. https://doi.org/10.1007/s11270-022-06031-8.

[9] Yu P, Han Y, Wang M, Zhu Z, Tong Z, Shao XY, Peng J, Hamid Y, Yang X, Deng Y, Huang Y. Heavy metal content and health risk assessment of atmospheric particles in China: a meta-analysis. Sci Total Environ 2023;867. https://doi.org/10.1016/j.scitotenv.2023.161556.

[10] Rivero CI-D, Fry KL, Gillings MM, Barlow CF, Aelion CM, Taylor MP. Sources, pathways and concentrations of potentially toxic trace metals in home environments. Environ Res 2023;220. https://doi.org/10.1016/j.envres.2022.115173.

[11] Rizo OD, Diaz AOC, Ramos AGT, Lopez DR. Heavy metals concentration, pollution indexes, and health risk assessment of urban road dust in the historical center of Havana, Cuba. Environ Monit Assess 2023;195. https://doi.org/10.1007/s10661-022-10875-2.

[12] Wang M, Lv Y, Lv X, Wang Q, Li Y, Lu P, Yu H, Wei P, Cao Z, An T. Distribution, sources and health risks of heavy metals in indoor dust across China. Chemosphere 2022;313. https://doi.org/10.1016/j.chemosphere.2022.137595.

[13] Obiora SC, Chukwu A, Davies TC. Contamination of the potable water supply in the lead – zinc mining communities of Enyigba, Southeastern Nigeria. Mine Water Environ 2019;38:148–57. https://doi.org/10.1007/s10230-018-0550-0.

[14] Andreas AL, Browser SS. Effects of lead and cadmium exposure on oxygen respiration rates of individual Antarctic foraminifera during agglutinated shell formation. J Exp Mar Biol Ecol 2021;537. https://doi.org/10.1016/j.jembe.2021.151514.

[15] Kumar V, Pandita S, Sidhu GPS, Sharma A, Khanna K, Kaur P, Bali AS, Setia R. Copper bioavailability, uptake, toxicity and tolerance in plants: a comprehensive review. Chemosphere 2021;262. https://doi.org/10.1016/j.chemosphere.2020.127810.

[16] Kumar A, Kumar A, Cabral-Pinto M, Chaturvedi AK, Shabnam AA, Subrahmanyam G, Mondal R, Gupta DK, Malyan SK, Kumar SS, Khan SA, Yadav KK. Lead toxicity: health hazards, influence on food chain, and sustainable remediation approaches. Int J Environ Res Publ Health 2020;17. https://doi.org/10.3390/ijerph17072179.

[17] Can H, Ozyigit II, Can M, Hocaoglu-Ozyigit A, Yalcin IE. Environment-based impairment in mineral nutrient status and heavy metal contents of commonly consumed leafy vegetables marketed in Kyrgyzstan: a case study for health risk assessment. Biol Trace Elem Res 2020;199:1123–44. https://doi.org/10.1007/s12011-020-02208-6.

[18] Sabry MIE, Stino FKR, El-Ghany WAA. Copper: benefits and risks for poultry, livestock, and fish production. Trop Anim Health Prod 2021;53. https://doi.org/10.1007/s11250-021-02915-9.

[19] Ma C, Liu F, Xie P, Zhang K, Yang J, Zhao J, Zhang H. Mechanism of Pb absorption in wheat grains. J Hazard Mater 2021;415. https://doi.org/10.1016/j.jhazmat.2021.125618.

[20] Aalami AH, Hoseinzadeh M, Manesh PH, Sharahi AJ, Aliabadi EK. Carcinogenic effects of heavy metals by inducing dysregulation of microRNAs: a review. Mol Biol Rep 2022;49:12227–38. https://doi.org/10.1007/s11033-022-07897-x.

[21] Wang C-C, Zhang Q-C, Kang S-G, Li M-Y, Zhang M-Y, Xu W-M, Xiang P, Ma LQ. Heavy metal(loid)s in agricultural soil from main grain production regions of China: bioaccessibility and health risks to humans. Sci Total Environ 2023;858. https://doi.org/10.1016/j.scitotenv.2022.159819.

[22] Elstrott B, Khan L, Olson S, Raghunathan V, DeLoughery T, Shatzel JJ. The role of iron repletion in adult iron deficiency anemia and other diseases. Eur J Haematol 2020;104:153–61. https://doi.org/10.1111/ejh.13345.

[23] Tsang T, Davis CI, Brady DC. Copper biology. Curr Biol 2021;31:421–7. https://doi.org/10.1016/j.cub.2021.03.054.

[24] De Souza ID, De Andrade AS, Dalmolin RJS. Lead-interacting proteins and their implication in lead poisoning. Crit Rev Toxicol 2018;48:375–86. https://doi.org/10.1080/10408444.2018.1429387.

[25] Wang X, Shen C, Zhou C, Bu Y, Yan X. Methods, principles and applications of optical detection of metal ions. Chem Eng J 2021;417. https://doi.org/10.1016/j.cej.2021.129125.

[26] Saleema M, Lee KH. Optical sensor: a promising strategy for environmental and biomedical monitoring of ionic species. RSC Adv 2015;5:72150–287. https://doi.org/10.1039/C5RA11388A.

[27] You L, Zha D, Anslyn EV. Recent advances in supramolecular analytical chemistry using optical sensing. Chem Rev 2015;115:7840–92. https://doi.org/10.1021/cr5005524.

[28] Wu J, Kwon B, Liu W, Anslyn EV, Wang P, Kim JS. Chromogenic/Fluorogenic ensemble chemosensing systems. Chem Rev 2015;115:7893–943. https://doi.org/10.1021/cr500553d.

[29] Sharma H, Kaur N, Singh A, Kuwar A, Singh N. Optical chemosensors for water sample analysis. J Mater Chem C 2016;4:5154–94. https://doi.org/10.1039/C6TC00605A.

[30] Ajay PVS, Printo J, Kiruba DSCG, Susithra L, Takatoshi K, Sivakumar M. Colorimetric sensors for rapid detection of various analytes. Mater Sci Eng C 2017;78:1231–45. https://doi.org/10.1016/j.msec.2017.05.018.

[31] Dongare PR, Gore AH. Recent advances in colorimetric and fluorescent chemosensors for ionic species: design, principle and optical signaling mechanism. ChemistrySelect 2021;6:5657–69. https://doi.org/10.1002/slct.202101090.

[32] Kramer J, Kang R, Grimm LM, De Cola L, Picchetti P, Biedermann F. Molecular probes, chemosensors, and nanosensors for optical detection of biorelevant molecules and ions in aqueous media and biofluids. Chem Rev 2022;122:3459–636. https://doi.org/10.1021/acs.chemrev.1c00746.

[33] Chen Z, Zhang Z, Qi J, You J, Ma J, Chen L. Colorimetric detection of heavy metal ions with various chromogenic materials: strategies and applications. J Hazard Mater 2023;441. https://doi.org/10.1016/j.jhazmat.2022.129889.

[34] McCrackena KE, Yoon J-Y. Recent approaches for optical smartphone sensing in resource-limited settings: a brief review. Anal Methods 2016;8:6591–601. https://doi.org/10.1039/C6AY01575A.

[35] Rezazadeh M, Seidi S, Lid M, Pedersen-Bjergaard S, Yamini Y. The modern role of smartphones in analytical chemistry. Trends Anal Chem 2019;118:548–55. https://doi.org/10.1016/j.trac.2019.06.019.

[36] Di Nonno S, Ulber R. Smartphone-based optical analysis systems. Analyst 2021;146:2749–68. https://doi.org/10.1039/D1AN00025J.

[37] Sivakumar R, Lee NY. Recent progress in smartphone-based techniques for food safety and the detection of heavy metal ions in environmental water. Chemosphere 2021;275. https://doi.org/10.1016/j.chemosphere.2021.130096.

[38] Mistlberger G, Crespo GA, Bakker E. Ionophore-based optical sensors. Annu Rev Anal Chem 2014;7:483–512. https://doi.org/10.1146/annurev-anchem-071213-020307.

[39] Xie X, Bakker E. Ion selective optodes: from the bulk to the nanoscale. Anal Bioanal Chem 2015;407:3899–910. https://doi.org/10.1007/s00216-014-8413-4.

[40] Mikhelson KN, Peshkova MA. Advances and trends in ionophore-based chemical sensors. Russ Chem Rev 2015;84:555–78. https://doi.org/10.1070/RCR4506.

[41] Du X, Xie X. Ion-Selective optodes: alternative approaches for simplified fabrication and signaling. Sensor Actuator B Chem 2021;335. https://doi.org/10.1016/j.snb.2020.129368.

[42] Oehme I, Wolfbeis OS. Optical sensors for determination of heavy metal ions. Microchim Acta 1997;126:177–92. https://doi.org/10.1007/BF01242319.

[43] Baldini F, Falai A. Characterization of an optical fibre pH sensor with methyl red as optical indicator. In: Martellucci S, Chester AN, Mignani AG, editors. Optical Sensors and Microsystems: New Concepts, Materials, Technologies. New York: Kluwer Academic Publishers; 2000. p. 53–60. https://doi.org/10.1007/0-306-47099-3_5.

[44] Enke D, Janowski F, Schwieger W. Porous glasses in the 21st century—a short review. Microporous Mesoporous Mater 2003;60:19–30. https://doi.org/10.1016/S1387-1811(03)00329-9.

[45] Ma QJ, Li HP, Yang F, Zhang J, Wu XF, Bai Y, Li XF. A fluorescent sensor for low pH values based on a covalently immobilized rhodamine–napthalimide conjugate. Sensor Actuator B Chem 2012;166–7:68–74. https://doi.org/10.1016/j.snb.2011.12.025.

[46] Muller R, Anders N, Titus J, Enke D. Ultra-thin porous glass membranes — an innovative material for the immobilization of active species for optical chemosensors. Talanta 2013;107:255–62. https://doi.org/10.1016/j.talanta.2012.12.038.

[47] Dalfen I, Borisov SM. Porous matrix materials in optical sensing of gaseous oxygen. Anal Bioanal Chem 2022;414:4311–30. https://doi.org/10.1007/s00216-022-04014-6.

[48] Galiński B, Chojnacki J, Wagner-Wysiecka E. Simple colorimetric copper(II) sensor – spectral characterization and possible applications. Spectrochim Acta Mol Biomol Spectrosc 2023;293. https://doi.org/10.1016/j.saa.2023.122472.

[49] Ghorbanian M, Asghari S, Tajbakhsh M. A new benzothiazole azo dye colorimetric chemosensor for detecting Pb^{2+} ion. Spectrochim Acta Mol Biomol Spectrosc 2023;296. https://doi.org/10.1016/j.saa.2023.122652.

[50] Luboch E, Bilewicz R, Kowalczyk M, Wagner-Wysiecka E, Biernat JF. Azo macrocyclic compounds. Adv Supramol Chem 2003;9:71–162.

[51] Wagner-Wysiecka E, Łukasik N, Biernat JF, Luboch E. Azo group(s) in selected macrocyclic compounds. J Inclusion Phenom Macrocycl Chem 2018;90:189–257. https://doi.org/10.1007/s10847-017-0779-4.

[52] Mortensen KT, Osberger TJ, King TA, Sore HF, Spring DR. Strategies for the diversity - oriented synthesis of macrocycles. Chem Rev 2019;119:10288–317. https://pubs.acs.org/doi/10.1021/acs.chemrev.9b00084.

[53] Amrhein JA, Knapp S, Hanke T. Synthetic opportunities and challenges for macrocyclic kinase inhibitors. J Med Chem 2021;64:7991–8009. https://doi.org/10.1021/acs.jmedchem.1c00217.

[54] Zhang X, Lin L, Li J, Duan S, Long Y, Li J. Recent progress in the synthesis of medium-sized ring and macrocyclic compounds. Chin J Org Chem 2021;41:1878–87. https://doi.org/10.6023/cjoc202010026.

[55] Wagner-Wysiecka E, Luboch E, Kowalczyk M, Biernat JF. Chromogenic macrocyclic derivatives of azoles-synthesis and properties. Tetrahedron 2003;59:4415–20. https://doi.org/10.1016/S0040-4020(03)00618-5.
[56] Luboch E, Wagner-Wysiecka E, Fainerman-Melnikova M, Lindoy LF, Biernat JF. Pyrrole azocrown ethers. Synthesis, complexation, selective lead transport and ion-selective membrane electrode studies. Supramol Chem 2006;18:593–601. https://doi.org/10.1080/10610270600879068.
[57] Wagner-Wysiecka E, Rzymowski T, Fonari MS, Kulmaczewski R, Luboch E. Pyrrole azocrown ethers-synthesis, crystal structures, and fluorescence properties. Tetrahedron 2011;67:1862–72. https://doi.org/10.1016/j.tet.2011.01.027.
[58] Wagner-Wysiecka E, Luboch E, Fonari MS. The synthesis, X-ray structure and metal cation complexation properties of colored crown with two heterocyclic residues as a part of macrocycle. Pol J Chem 2008;82:1319–30.
[59] Wagner-Wysiecka E, Jamrógiewicz M, Fonari MS, Biernat JF. Azomacrocyclic derivatives of imidazole: synthesis, structure, and metal ion complexation properties. Tetrahedron 2007;63:4414–21. https://doi.org/10.1016/j.tet.2007.03.095.
[60] Galiński B, Luboch E, Chojnacki J, Wagner-Wysiecka E. Novel diazocrowns with pyrrole residue as lead(II) colorimetric probes. Materials 2021;14. https://doi.org/10.3390/ma14237239.
[61] Galiński B, Wagner-Wysiecka E. Pyrrole bearing diazocrowns: selective chromoionophores for lead(II) optical sensing. Sensor Actuator B Chem 2022;361. https://doi.org/10.1016/j.snb.2022.131678.
[62] Jamrógiewicz M, Kledzik K, Gwiazda M, Wagner-Wysiecka E, Jezierska J, Biernat JF, Kłonkowski A. Optical recognition elements: macrocyclic imidazole chromoionophores entrapped in silica xerogel. Mater Sci-Pol 2007;25:1044–51.
[63] Dolomanov OV, Bourhis LJ, Gildea RJ, Howard JAK, Puschmann H. OLEX2: a complete structure solution, refinement and analysis program. J Appl Crystallogr 2009;42:339–41. https://doi.org/10.1107/S0021889808042726.
[64] Sheldrick GM. Shelxt - integrated space-group and crystal-structure determination. Acta Crystallogr A 2015;71:3–8. https://doi.org/10.1107/S2053273314026370.
[65] Koziskova J, Hahn F, Richter J, Kozisek J. Comparison of different absorption corrections on the model structure of tetrakis(m_2-acetato)-diaqua-di-copper(II). Acta Chim Slovaca 2016;9:136–40. https://doi.org/10.1515/acs-2016-0023.
[66] Dinten O, Spichiger UE, Chaniotakis N, Gehrig P, Rusterholz B, Morf WE, Simon W. Lifetime of neutral-carrier-based liquid membranes in aqueous samples and blood and the lipophilicity of membrane components. Anal Chem 1991;63:596–603. https://doi.org/10.1021/ac00006a009.
[67] Kyvala M, Lukes I. Program package "OPIUM" (free access) at, https://web.natur.cuni.cz/~kyvala/opium.html.
[68] Abramoff MD, Magalhaes PJ, Ram SJ. Image processing with ImageJ. Biophot Int 2004;11:36–42.
[69] Schneider CA, Rasband WS, Eliceiri KW. NIH Image to ImageJ: 25 years of image analysis. Nat Methods 2012;9:671–5. https://doi.org/10.1038/nmeth.2089.
[70] Gavrilenko NA, Muravyov SV, Silushkin SV, Spiridonovab AS. Polymethacrylate optodes: a potential for chemical digital color analysis. Measurement 2014;51:464–9. https://doi.org/10.1016/j.measurement.2013.11.027.
[71] Job P. Formation and stability of inorganic complexes in solution. Ann Chim 1928;9:113–203.
[72] Shahamirifard SA, Ghaedi M, Montazerozohori M. Design a sensitive optical thin film sensor based on incorporation of isonicotinohydrazide derivative in sol–gel matrix for determination of trace amounts of copper (II) in fruit juice: effect of sonication time on immobilization approach. Ultrason Sonochem 2018;42:723–30. https://doi.org/10.1016/j.ultsonch.2017.12.043.
[73] Parsaeea Z, Karachi N, Razavi R. Ultrasound assisted fabrication of a novel optode base on a triazine based Schiff base immobilized on TEOS for copper detection. Ultrason Sonochem 2018;47:36–46. https://doi.org/10.1016/j.ultsonch.2018.04.007.
[74] Kumar SK, Mohan AM. Porous inorganic/organic hybrid monolith-based solid sensor for the colorimetric analysis of Cu^{2+} ions. J Nanoparticle Res 2021;23. https://doi.org/10.1007/s11051-021-05316-z.
[75] Salman S, Hasan N, Hasan M, Kubra KT, Sheikh C, Rehan AI, Waliullah RM, Rasee AI, Awua E, Hossain MS, Alsukaibi AKD, Alshammari HM, Awual R. Improving copper(II) ion detection and adsorption from wastewater by the ligand-functionalized composite adsorbent. J Mol Struct 2023:1282. https://doi.org/10.1016/j.molstruc.2023.135259.
[76] Awual R, Hasan M. Novel conjugate adsorbent for visual detection and removal of toxic lead(II) ions from water. Microporous Mesoporous Mater 2014;196:261–9. https://doi.org/10.1016/j.micromeso.2014.05.021.
[77] Prabhakaran D, Subashini C, Maheswari MA. Synthesis of mesoporous silica monoliths — a novel approach towards fabrication of solid-state optical sensors for environmental applications. Int J Nanosci 2016;15. https://doi.org/10.1142/S0219581X16600140.
[78] Nur Y, Rohaeti E, Darusman LK. Optical sensor for the determination of Pb(II) based on immobilization of dithizone onto chitosan-silica membrane. Indones J Chem 2017;17:7–14. https://doi.org/10.22146/ijc.23560.
[79] Awual R. Mesoporous composite material for efficient lead(II) detection and removal from aqueous media. J Environ Chem Eng 2019;7. https://doi.org/10.1016/j.jece.2019.103124.